



# Effect of CuO doping on structural features, optical absorption and photoluminescence behavior of ZnO-based glasses

S. Ibrahim<sup>1</sup>, Y. M. Hamdy<sup>2</sup>, H. Darwish<sup>1</sup>, and A. A. Ali<sup>1,\*</sup>

<sup>1</sup>Glass Research Department, National Research Centre, El-Buhouth St, Dokki, Cairo 12622, Egypt

<sup>2</sup>Spectroscopy Department, National Research Center, El-Buhouth St, Dokki, Cairo 12622, Egypt

Received: 2 January 2023

Accepted: 14 March 2023

Published online:

6 April 2023

© The Author(s) 2023

## ABSTRACT

Glasses composed of ZnO–SiO<sub>2</sub>–B<sub>2</sub>O<sub>3</sub>–In<sub>2</sub>O<sub>3</sub> with the addition of different content of CuO were prepared by a popular melt–quenching methodology. The effect of the addition of copper oxide in the glass network was investigated using density, FTIR spectroscopy, optical absorption, and photoluminescence spectroscopy. By increasing the concentration of CuO, a decrease in the density is observed, indicating structural changes in the glass network. The structural building units of glasses are BO<sub>3</sub>, BO<sub>4</sub>, and ZnO<sub>4</sub> according to the FTIR spectra. The absorption spectra of these glasses reveal a distinct broad band at 744 nm due to <sup>2</sup>B<sub>1g</sub> → <sup>2</sup>B<sub>2g</sub> characteristic transition of cupric ion in the distorted octahedral sites. The optical band gap energies (*E<sub>g</sub>*) and refractive indices of the studied glasses were also evaluated using the ASF, DASF, and Tauc techniques which revealed that (*E<sub>g</sub>*) values are in gradual decrease with a rise content of CuO. The photoluminescence analysis including emission and CIE chromaticity of the prepared samples were carried out. The emission spectra supported divalent state of copper ions in a distorted octahedral geometry of the glass network upon UV excitation at 270 nm. These results may suggest the material of glass as a potential candidate in the photonics applications.

## 1 Introduction

Zinc borate glasses are of technological importance because they can be used in a variety of electronic products since of their low melting temperatures. In the area of electric equipment, like in multi-layer ceramic capacitors, electric cathode ray tubes, modules plasma display panels, low-temperature co-fired

ceramics (LTCC), low melting glasses are often used [1–3].

Zinc oxide is a glass modifier that breaks BOB linkages and introduces coordinated defects called as dangling bonds, as well as non-bridging oxygen (NBO) atoms into the glass matrix; in this case, Zn<sup>2+</sup> is octahedral coordinated. ZnO may take part in the glass matrix with ZnO<sub>4</sub> structural units whenever

Address correspondence to E-mail: ali\_nrc@hotmail.com

zinc is connected to four oxygen ions in a covalent bond form. The network structure in this instance is assumed to be made up of  $\text{ZnO}_4$  and  $\text{BO}_4$  pyramidal units connected by B–O–Zn bonds [4, 5]. The addition of zinc to the borate glass system improves its durability, strength, optical functionalization, and electron emission capacity, making it suitable for a variety of applications [6, 7].

Transition metal ions (TMIs)-doped glasses have received much interest in recent years due to their photoconducting and memory properties. They are also found in fiber optic communication systems, solid state lasers, and luminescent solar energy concentrators [8–10].

The copper atom's electron configuration is  $[\text{Ar}] 3d^{10}4s^0$ , and its stable ionic states are  $\text{Cu}^+$  and  $\text{Cu}^{2+}$ ; the cuprous ion does not create coloring because its five d-orbitals are filled, whereas cupric ions produce color centers with absorption bands in the visible wavelength region [11], resulting in materials with attractive blue and sometimes green color. The color of the glasses is determined by the  $\text{Cu}^{2+}$  content, its specific coordination, composition, and basicity [12].

The  $\text{Cu}^{2+}$  state glass network is expected to have the most copper ions. During the melting and annealing processes, however, copper ions can be oxidized or reduced from  $\text{Cu}^{2+}$  to  $\text{Cu}^{3+}$  and  $\text{Cu}^+$ .  $\text{Cu}^{2+}$  ions are found in octahedral sites in the glass network, while  $\text{Cu}^+$  and  $\text{Cu}^{3+}$  ions are found in tetrahedral places [13, 14]. Copper-containing glasses have a number of attractive features that cover a broad range of applications such as lighting [15], nonlinear optics [16], bandpass filters [17], spectral conversion in solar cells [18], and lasers [19].

The physical and optical properties of copper-doped glasses have been studied by a number of scientists. For example, Samir et al. [20] used the ternary  $30 \text{ Na}_2\text{O} - 20 \text{ ZnO} - 50 \text{ B}_2\text{O}_3$  and added  $\text{CuO}$  up to 7 mol% at the expense of  $\text{B}_2\text{O}_3$ . The possibility of adjusting the filtering effect has been offered [11] based on several physical property estimations and the evaluation of band gap and Urbach energies. Additionally, Zhang et al. [21] and Verwey et al. [22] have also investigated  $\text{Cu}_2\text{O}$ -doped  $\text{B}_2\text{O}_3/\text{BaO}/\text{Li}_2\text{O}/\text{La}_2\text{O}_3/\text{Al}_2\text{O}_3/\text{As}_2\text{O}_3$  and  $\text{SrB}_2\text{O}_7$  glasses, emphasizing on the luminescence caused by the existence of  $\text{Cu}^+$  ions. The use of  $\text{As}_2\text{O}_3$  with reductant characteristics in these kinds of works was assumed to be advantageous in avoiding  $\text{Cu}^+$  oxidation to  $\text{Cu}^{2+}$  and

therefore facilitating the evaluation of  $\text{Cu}^+$  photoluminescence in borate glasses. Okasha et al. [23] recently investigated the  $15\text{NaF} - 5 \text{ CaF}_2 - 80\text{B}_2\text{O}_3$  glass, for which  $\text{CuO}$  was added to 12 wt% instead of  $\text{B}_2\text{O}_3$  to make tunable glasses for optical filters. After many spectroscopic characterizations, optical band gap energies were determined and reported in a similar manner, with a decreasing trend.

The goal of this paper is to present results from UV/Vis, FTIR, and PL spectroscopies, as well as density measurements, on multicomponent  $\text{ZnO} - \text{SiO}_2 - \text{B}_2\text{O}_3 - \text{In}_2\text{O}_3$  glasses doped with  $\text{CuO}$ , and to study the effect of copper oxide concentration variation on them. These results pointed to glass as a possible candidate for photonics applications.

## 2 Experimental

The detailed chemical compositions of the glasses used in the present study are as follows:

- $\text{Cu}_1$ :  $65\text{ZnO} - 10\text{SiO}_2 - 23\text{B}_2\text{O}_3 - 2\text{In}_2\text{O}_3$ ,
- $\text{Cu}_2$ :  $65\text{ZnO} - 10\text{SiO}_2 - 23\text{B}_2\text{O}_3 - 2\text{In}_2\text{O}_3 - 0.005\text{CuO}$ ,
- $\text{Cu}_3$ :  $65\text{ZnO} - 10\text{SiO}_2 - 23\text{B}_2\text{O}_3 - 2\text{In}_2\text{O}_3 - 0.020\text{CuO}$ ,
- $\text{Cu}_4$ :  $65\text{ZnO} - 10\text{SiO}_2 - 23\text{B}_2\text{O}_3 - 2\text{In}_2\text{O}_3 - 0.035\text{CuO}$ ,
- $\text{Cu}_5$ :  $65\text{ZnO} - 10\text{SiO}_2 - 23\text{B}_2\text{O}_3 - 2\text{In}_2\text{O}_3 - 0.050\text{CuO}$ .

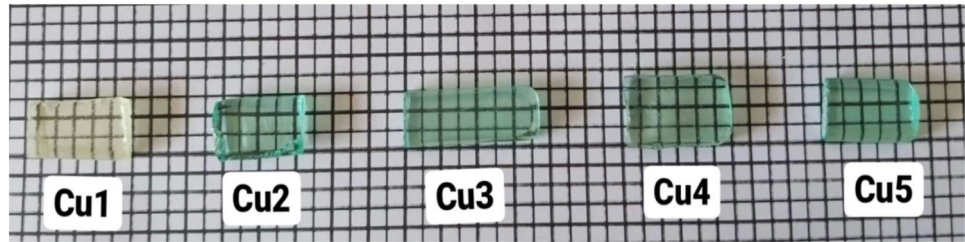
Appropriate amounts (all in mol%) of analytical grade reagents of  $\text{ZnO}$ ,  $\text{SiO}_2$ ,  $\text{H}_3\text{BO}_3$ ,  $\text{In}_2\text{O}_3$ , and  $\text{CuO}$  were used. Appropriate amounts of chemicals were grinded and mixed in an agate mortar and the batch were placed in porcelain crucibles and then melted in an electrical furnace at  $1100^\circ\text{C}$  for 2 h till a bubble-free liquid was formed. The resultant bubble-free melt was then poured on stainless steel plates. The samples were immediately transferred to annealing furnace at  $400^\circ\text{C}$  for half an hour then it was switched off and left to cool to ambient temperature. The photographs of transparent samples synthesized and without any treatments are shown in Fig. 1. All the samples contain  $\text{CuO}$  showed blue color.

Archimedes method is used to estimate the density ( $\rho$ ) of the prepared samples at room temperature by using deionized water as immersion liquid [24].

$$\rho \left\{ \frac{W_1}{W_1 - W_2} \right\} \times \rho_{\text{water}}, \quad (1)$$

where  $W_1$  is the weight of sample in air,  $W_2$  is the weight of sample in water, and  $\rho_{\text{water}}$  is the density of water ( $\rho_{\text{water}} = 0.9977 \text{ g/cm}^3$ ).

**Fig. 1** A picture of glass samples



FTIR spectra were obtained in the wavenumber range of 400–4000  $\text{cm}^{-1}$  using Nicolet™ iS™ 10 FTIR Spectrometer. Each sample was mixed with KBr by the ratio 1:100 in weight and then pressed to produce a homogeneous pellet. The infrared absorbance measurements were carried out at room temperature and immediately after preparing the pellets to avoid moisture.

UV–Vis spectra were recorded on these samples at room temperature using a Cary series UV/Vis-spectrophotometer within a wavelength of 200–1100 nm in the absorption mode.

The photoluminescence spectra were recorded under UV excitation using a fluorescence spectrometer (Type JASCO FP-6500, Japan) equipped with a xenon flash lamp at the excitation light source. The scan speed is 0.1 s/step with a step length of 0.25 nm and a slit width of 0.2 nm. The CIE1931 chromaticity diagram was applied to identify the emitted color from light sources using three dimension-less quantities  $\bar{x}(\lambda)$ ,  $\bar{y}(\lambda)$ , and  $\bar{z}(\lambda)$ . The tristimulus values for a non-monochromatic light source with spectral relative power  $P(\lambda)$  are given by

$$X = \int P(\lambda)\bar{x}(\lambda)d\lambda, \tag{2}$$

$$Y = \int P(\lambda)\bar{y}(\lambda)d\lambda, \tag{3}$$

$$Z = \int P(\lambda)\bar{z}(\lambda)d\lambda, \tag{4}$$

where  $X$ ,  $Y$ , and  $Z$  are the tristimulus values that identify the three primary light colors red, green, and blue that needed to match the color  $P(\lambda)$  and from the tristimulus values the color chromaticity coordinates  $x$  and  $y$  can be determined using the following expression [25–27]:

$$x = \frac{X}{X + Y + Z}, \tag{5}$$

$$y = \frac{Y}{X + Y + Z}, \tag{6}$$

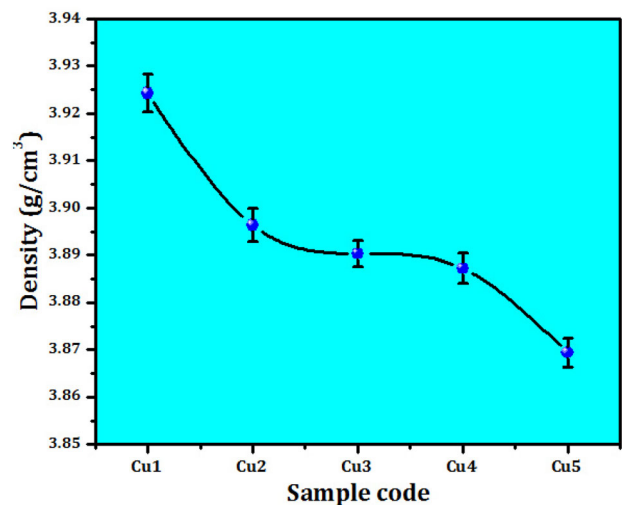
$$z = \frac{Z}{X + Y + Z}. \tag{7}$$

### 3 Results and discussion

#### 3.1 Density

It is well known that density is a property which can be used for determining rigidity and changes in the structure of the material. Changes in geometrical structure, crosslink density, coordination number, structural softness, and interstitial spaces distances in glass matrix are all the factors that influence it [28]. The variation of density values of the studied glass samples is presented in Fig. 2. The addition of CuO to base glass sample leads to decrease the density values (Table 1).

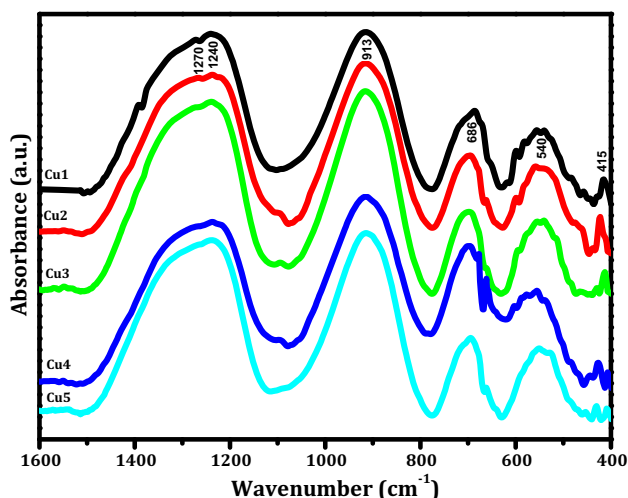
As the amount of the CuO modifier increases, structural changes including the conversion of  $\text{BO}_4$  tetrahedral structural units into  $\text{BO}_3$  trigonal



**Fig. 2** Density of the glasses ZnO–SiO<sub>2</sub>–B<sub>2</sub>O<sub>3</sub>–In<sub>2</sub>O<sub>3</sub>:CuO

**Table 1** Density and optical band gap energies obtained with Tauc, ASF, and DASF methods of the prepared glasses

Sample code	Density (g/cm <sup>3</sup> )	Optical band gap energy, $E_g$ (eV)				
		Tauc method		ASF method		DASF method
		$E_{\text{gap,Direct}}^{\text{Tauc}}$	$E_{\text{gap,Indirect}}^{\text{Tauc}}$	$E_{\text{gap,Direct}}^{\text{ASF}}$	$E_{\text{gap,Indirect}}^{\text{ASF}}$	$E_{\text{gap}}^{\text{DASF}}$
Cu <sub>1</sub>	3.9318	3.263	2.936	3.286	3.038	3.323
Cu <sub>2</sub>	3.9014	3.191	2.922	3.199	2.976	3.298
Cu <sub>3</sub>	3.892	3.168	2.919	3.174	2.926	3.274
Cu <sub>4</sub>	3.8736	3.146	2.905	3.149	2.877	3.224
Cu <sub>5</sub>	3.8474	3.127	2.887	3.124	2.852	3.199

**Fig. 3** Infrared absorption spectra of the prepared glasses

structural units occur. Accordingly, the addition of CuO to base glass changes the number of oxygens around B<sup>3+</sup> and Zn<sup>2+</sup> cations, leads to creation of BO<sub>3</sub> and ZnO<sub>4</sub> structural units [29].

### 3.2 FTIR analysis

Infrared spectroscopy is commonly employed to get important information on the arrangement of structural units in the prepared glasses. It is well known that the vibrations of specific structural units in the network of glass are believed to be independent of vibrations of any other units in the network [30]. The overall spectrum is made up of several absorption bands that extend from 400 to 1600 cm<sup>-1</sup> and are centered in the mid-region. Figure 3 shows IR spectra of the examined glasses doped with various amounts of copper ion. Three traditional broad bands are identified because of borate family [31–33]: (1) 1st groups are ranged from 1200 to 1600 cm<sup>-1</sup>, which are attributed to the presence of BO<sub>3</sub> units, i.e., the

asymmetric stretching relaxation of the B–O bonds; (2) 2nd groups are ranged from 800 to 1200 cm<sup>-1</sup>, which may be due to presence of BO<sub>4</sub> units, i.e., the B–O bond stretching of BO<sub>4</sub> groups; (3) the last groups are ranged from 625 to 725 cm<sup>-1</sup> due to the presence of bending B–O linkages.

The infrared absorption spectrums of the glass free CuO (Fig. 3) showed five absorption bands centered around 1270, 1240, 913, 686, and 415 cm<sup>-1</sup>. The weak band around 1270 can be attributed to the presence of meta-borate chains [30]. The appearance of absorption band at 1240 cm<sup>-1</sup> may be due to the asymmetric stretching vibrations of B–O bonds in BO<sub>3</sub> units, from pyro- and *ortho*-borate groups, which characterized by presence of a large number of NBOs. As shown in Fig. 3, the addition of CuO leads to increase in the relative area of 1240 cm<sup>-1</sup> band and this behavior indicates that the addition of CuO increases the amount of NBOs in great agreement with the formation of octahedral coordinated copper ion [34, 35].

The appearance of the band around at 913 cm<sup>-1</sup> may be due to the stretching vibrations of BO<sub>4</sub> units in different structural units [36]. The absorption band ~690 cm<sup>-1</sup> may be due to the presence of B–O–B bending vibrations of borate network [37, 38] or/and the vibrated oxygen which connect the two trigonal boron atoms [39]. With increasing copper ion content, the relative area of this band increases and shifts to higher wavenumbers. The Cu<sup>2+</sup> ions' electrostatic field could be responsible for this shift [40]. The increasing of CuO content, causing a rise in the electron cloud density surrounding the oxygen in the BO<sub>3</sub> unit, leads to an increase in the B–O–B band's roll-torque and, as a result, a shift toward higher wavenumbers. Because of the generated electrostatic field, which weakens the borate network, this action creates additional new B–O–Cu bridge bonds [40].



Generally, the boroxol ring in the borate glass network is usually attributed to the IR absorption band at  $806\text{cm}^{-1}$ . The peak at  $806\text{cm}^{-1}$  is missing in this study, indicating that there is no boroxol ring in the glass network. With the addition of CuO into base glass and with increasing its concentration the band due to  $\text{BO}_4$  units is observed to shift toward higher wavenumber and its intensity decreases, whereas the center of  $\text{BO}_3$  groups is shifted to lower wavenumber and its intensity increases. The appearance of bands the range  $400\text{--}600\text{cm}^{-1}$  is due to the presence of ZnO which forms Zn–O tetrahedral bending vibrations in the current glass system [41]. It is well known that ZnO is consider as a glass modifier which breaks B–O–B bonds and then enters the glass network (usually, the oxygen in ZnO breaks local symmetry while  $\text{Zn}^{2+}$  ions occupy interstitial sites) and introducing coordination defects known as dangling bonds, as well as NBO ions. Zinc oxide may also contribute to the glass matrix with  $\text{ZnO}_4$  structural groups when  $\text{Zn}^{2+}$  is joined to four oxygens in a covalence bond configuration [42, 43]. The intensity of the band due to  $\text{ZnO}_4$  units is highest in the spectrum of the glass code  $\text{Cu}_1$  and lowest in the spectrum of the glass code  $\text{Cu}_5$ . Copper ions operate as modifiers, causing bonding defects by disrupting the bonds B–O–B, B–O–Zn, etc. [44]. With the addition of CuO in glass matrix suggests an increase in copper ions content participating in network position modification and the change of  $\text{BO}_4$  groups to  $\text{BO}_3$  groups in the glass matrix.

The deconvoluted spectra of all glass samples are made to obtain N4. The fraction of four coordinated boron was calculated using the relative areas corresponding to  $\text{BO}_3$  and  $\text{BO}_4$  vibrational groups. Sample  $\text{Cu}_3$  spectra are given as an example of the deconvoluted spectral data (Fig. 4). Calculated values of N4 are as follows:

$$N4 = \frac{A4}{A3 + A4},$$

where A3 and A4 are the relative areas corresponding to  $\text{BO}_3$  and  $\text{BO}_4$  structural units, respectively.

The values of N4 are 0.431, 0.425, 0.415, 0.402, and 0.392 for sample from  $\text{Cu}_1$  to  $\text{Cu}_5$ , respectively. The values of N4 decreased with increasing the concentration of CuO this is due to the structural changes involving the conversions of the  $\text{BO}_4$  into  $\text{BO}_3$  structural units as the content of the CuO glass modifier increases.

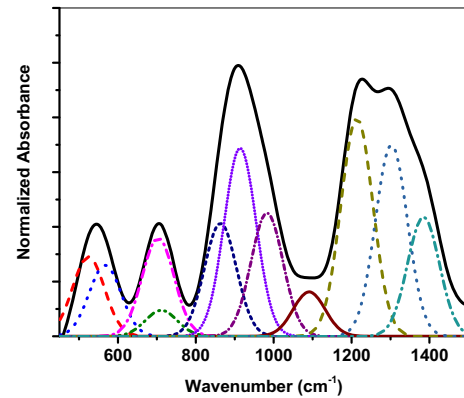


Fig. 4 Deconvoluted spectra of  $\text{Cu}_3$  glass

### 3.3 Analysis of ultraviolet and visible (UV–Vis) spectrum

The study of optical absorption in glasses has helped to understand electronic band structure and optical transitions in these materials. Depending on their valence state and coordination number, and hence their d level state, TMIs have a wide range of optical absorption spectra in the UV–Vis range. [29].

The optical absorption spectra of the prepared glasses are presented in Fig. 5. The edge of absorption ( $\lambda_c$ ) is red-shifted as the CuO content increases from  $\sim 396\text{nm}$  in  $\text{Cu}_1$  to  $\sim 410\text{nm}$  in  $\text{Cu}_5$ . With increasing amounts of CuO, the cutoff wavelength ( $\lambda_c$ ) increases, indicating an increase in octahedral  $\text{Cu}^{2+}$  ions. This behavior indicates that the band gap energy  $E_g$  values decreased due to the doping of varying content of CuO inside the glass network. As a result, electrons can migrate from the valance to the conduction band, resulting in charge flow [45].

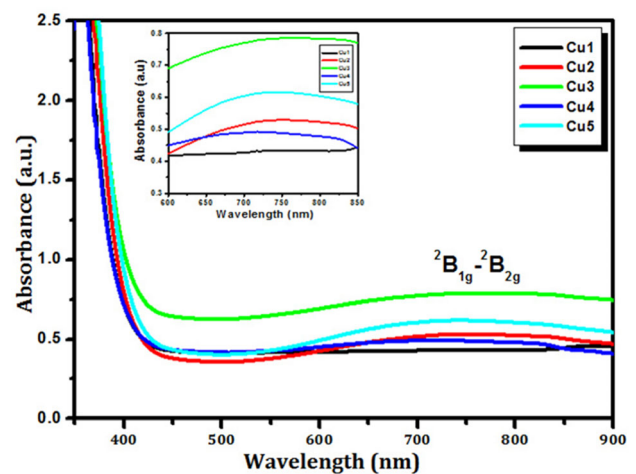


Fig. 5 Optical absorption spectra of the prepared glasses

Further, copper can be present in glasses as  $\text{Cu}^{2+}$  and  $\text{Cu}^+$  ions. In the UV–Vis range,  $\text{Cu}^+$  ions exhibit no absorption, but  $\text{Cu}^{2+}$  ions have a significant absorption [46].

The  $3d^9$  electronic configuration of  $\text{Cu}^{2+}$  ions has a two-dimensional (2D) ground state. The 2D states are separated into  $e_g$  and  $t_{2g}$  energy levels in the octahedron crystal field. The  $e_g$  levels are divided into  ${}^2B_{1g}$  and  ${}^2A_{1g}$ , whereas the  $t_{2g}$  levels are divided into  ${}^2B_{2g}$  and  ${}^2E_g$ . The ground state of these is  $B_{1g}$ . As a result, copper ions are expected to have three bands related to the transitions of  ${}^2B_{1g} \rightarrow {}^2A_{1g}$ ,  ${}^2B_{1g} \rightarrow {}^2B_{2g}$ , and  ${}^2B_{1g} \rightarrow {}^2E_g$  [47–49].

The overlap of the three transitions was interpreted as a single optical absorption band, as shown in Fig. 5. The absorbance peak was centered at 744 nm due to the transition of  $\text{Cu}^{2+}$  ions into distorted octahedral sites from  ${}^2B_{1g} \rightarrow B_{2g}$ .

### 3.4 Determination of optical band gap energy

In the nanomaterials industries and semiconductor, measuring the band gap energy is important. Tauc [50], Mott and Davis [51] explored the energy band gaps associated to optical energy. Souri and Shomalian [52], Souri and Tahan [53], and Alarcon et al. [54] used the absorbance spectrum fitting (ASF) approach to estimate optical band gaps, besides Souri and Tahan [53] and Ali et al. [55] used the first derivation of the absorption spectrum fitting method to evaluate optical band gaps (DASF). The optical energy of the glasses under investigation was estimated using the following methods.

#### 3.4.1 Tauc's method ( $E_{\text{gap}}^{\text{Tauc}}$ )

The Tauc method [50] has traditionally been used to estimate band gap energies in crystalline and amorphous semiconductors in most of the investigations.

One of the most important parameters for estimating the band gap energy is the optical absorption coefficient ( $\alpha$ ) and whether the band structure has changed, and it is a material's ability to absorb light at a specific wavelength [56]. When evaluating materials of different thicknesses, the absorption coefficient is a good measure to use [57]:

$$\alpha = (2.303) \frac{A}{d}, \quad (8)$$

where  $A$  is the absorbance and  $d$  is the thickness of the sample. The optical band gap of glass samples can be determined using the following formula [58]:

$$\alpha(h\nu) = B(h\nu - E_{\text{gap}}^{\text{Tauc}})^n, \quad (9)$$

where  $B$  is a constant and  $h\nu$  is the energy of the incident photon. The type of optical transition ( $n = 2, 1/2, 3, 1/3$ ) is represented by  $n$  for indirect allowed, direct allowed, forbidden indirect, and forbidden direct transitions [59]. Figures 6 and 7 show Tauc plots obtained from  $(\alpha h\nu)^{0.5}$  against  $h\nu$  and  $(\alpha h\nu)^2$  against  $h\nu$ , respectively. Extending the linear sections of plots to the X-axis, making  $(\alpha h\nu)^{0.5} = 0$  and  $(\alpha h\nu)^2 = 0$  yields the values of  $E_{\text{gap}}^{\text{Tauc}}$  of glasses (for allowed indirect and direct transitions). The optical band gap ( $E_{\text{gap}}^{\text{Tauc}}$ ) values are given by the intercept on the  $h\nu$  axis.

For allowed direct transitions, the obtained band gap values for the produced glasses decreased from 3.263 to 3.127 eV, and for allowed indirect transitions, they decreased from 2.936 to 2.887 eV as shown in Table 2.

The addition of CuO content has been found to decrease  $E_g$  values because it contributes additional defect states (such wrong bonds and color centers) into the matrix [60]. Also, there is some overlap between delocalized quasi-band states and localized d orbital of Cu states, which could result in major changes in optical excitation transfer. The concentration of these defects, and hence the CuO content, was found to be related to localized state density.

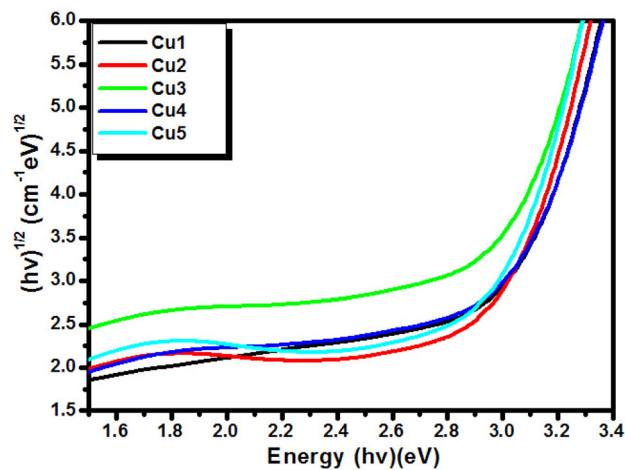


Fig. 6 Variation of  $(\alpha h\nu)^{0.5}$  with  $h\nu$  for  $\text{Cu}_1$ – $\text{Cu}_5$  glasses

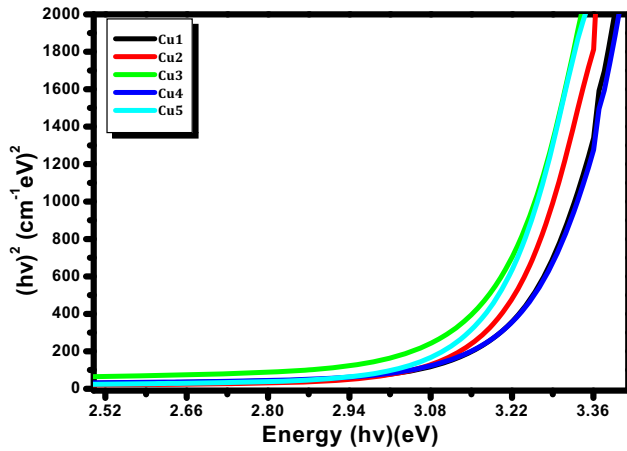


Fig. 7 Variation of  $(\alpha hv)^2$  with  $hv$  for Cu<sub>1</sub>–Cu<sub>5</sub> glasses

Color centers or wrong bonds localized states overlap and expand into the mobility gap, lowering  $E_g$ . Besides, BO<sub>3</sub> units containing NBOs atoms formed when the amount of Cu<sup>2+</sup> ions in the borate network increases. The band gap is shown to decrease as NBOs become more excited than bridging oxygens (BOs) [61].

3.4.2 Absorbance spectrum fitting method (ASF)

The optical band gap can also be estimated using the absorption spectrum fitting ( $E_{gap}^{ASF}$ ) method, as proposed by Souri and Shomalian [52] and Alarcon et al. [54], the  $\alpha(\nu)$  can be determined as a function of photon wavelength ( $\lambda$ ):

$$\alpha(\lambda) = C(hc)^{r-1} \lambda(\lambda^{-1} - \lambda_g^{-1})^r, \tag{10}$$

where  $h$ ,  $c$ ,  $\lambda_g$  express to the Plank’s constant, light velocity, and the wavelength corresponding to the optical band gap. Equation (10) can be rewritten as follows:

$$A(\lambda) = D\lambda(\lambda^{-1} - \lambda_g^{-1})^r, \tag{11}$$

where  $D = [C(hc)^{r-1} d/2.303]$ . Equation (11) demonstrates that the optical energy band gap could be estimated only from absorbance values, without need for a thick glass sample. Extension of the linear region of  $(A\lambda^{-1})^{r-1}$  versus  $(\lambda^{-1})$  at  $(A\lambda^{-1})^{r-1} = 0$  can be used to determine the  $\lambda_g$ . Figures 8 and 9 show the variation of  $(A\lambda^{-1})^{0.5}$  and  $(A\lambda^{-1})^2$  with  $(\lambda^{-1})$  for indirect and direct allowed transition, respectively. Moreover, Eq. (12) can be used to estimate the  $E_{gap}^{ASF}$  directly from  $\lambda_g$ :

$$E_{gap}^{ASF} = \frac{hc}{\lambda_g} = 1239.83 \times \lambda_g^{-1}. \tag{12}$$

When the CuO content increased, the indirect  $E_g$  of glass samples were decreased from 3.038 to 2.8520 eV and from 3.286 to 3.124 eV for direct  $E_g$ .

3.4.3 Derivation absorbance spectrum fitting method (DASF)

The optical band gap energies of the examined glasses were accurately determined using the DASF method [62, 63]. The band gap energy values were determined by the samples’ optical absorption, which inhibited the evaluation of sample thickness, compounding the estimation error [63]. The glasses’ optical absorbance ( $A$ ) can be represented as [53]

$$\ln\left(\frac{A(\lambda)}{\lambda}\right) = \ln(D) + r\ln(\lambda^{-1} - \lambda_g^{-1})^r, \tag{13}$$

$$\frac{d\{\ln(A(\lambda)\lambda^{-1})\}}{d(\lambda^{-1})} = \frac{r}{(\lambda^{-1} - \lambda_g^{-1})}. \tag{14}$$

As shown in Eq. (14), the value of  $\lambda_g$  should cause a discontinuity in the  $d\{\ln(A(\lambda)\lambda^{-1})\}$  against  $\lambda^{-1}$  graph

Table 2 Refractive index obtained with Tauc, ASF, and DASF methods of the prepared glasses

Sample code	Refractive index				
	Tauc method		ASF method		DASF method
	Direct	Indirect	Direct	Indirect	
Cu <sub>1</sub>	2.329	2.407	2.324	2.387	2.315
Cu <sub>2</sub>	2.347	2.418	2.347	2.404	2.321
Cu <sub>3</sub>	2.353	2.419	2.352	2.417	2.327
Cu <sub>4</sub>	2.358	2.423	2.358	2.431	2.340
Cu <sub>5</sub>	2.363	2.428	2.364	2.438	2.345

at  $\lambda^{-1} = \lambda_g^{-1}$ . Thus, the optical energy gap ( $E_{\text{gap}}^{\text{DASF}}$ ) values can be determined by using the following formula:

$$E_{\text{gap}}^{\text{DASF}} = \frac{hc}{\lambda_g} = \frac{1239.83}{\lambda_g} \quad (15)$$

The dependence of  $d\{\ln(A(\lambda)\lambda^{-1})\}$  on  $(\lambda^{-1})$  for the proposed glasses (Cu<sub>1</sub> to Cu<sub>5</sub>) is represented in Fig. 10.  $E_{\text{gap}}^{\text{DASF}}$  values for the present glasses were calculated using Eq. (15) are listed in Table 1.  $E_{\text{gap}}^{\text{DASF}}$  values decrease from 3.323 to 3.194 eV.

The  $E_{\text{gap}}^{\text{DASF}}$  values found were very similar to the ASF and Tauc values. Table 1 shows all the optical energy band gap values for the produced glasses using various models.

Using the DASF, ASF, and Tauc techniques, the CuO content-dependent energy band gaps of the studied glasses were calculated. The results (Fig. 11; Table 1) showed that when the CuO content in the glass network increased, the values of  $E_g$  for both direct and indirect optical transitions decreased. The creation of more NBO in the highest valence band allowed the NBO to move to the conduction band, decreasing the glasses'  $E_g$  values.

#### 3.4.4 Refractive index

The optical refractive index ( $n$ ) determines the application of the investigated glasses in various optical applications. As a result,  $n$  was determined for all glasses in this investigation. In Tauc's, ASF, and DASF techniques, the refractive index in direct

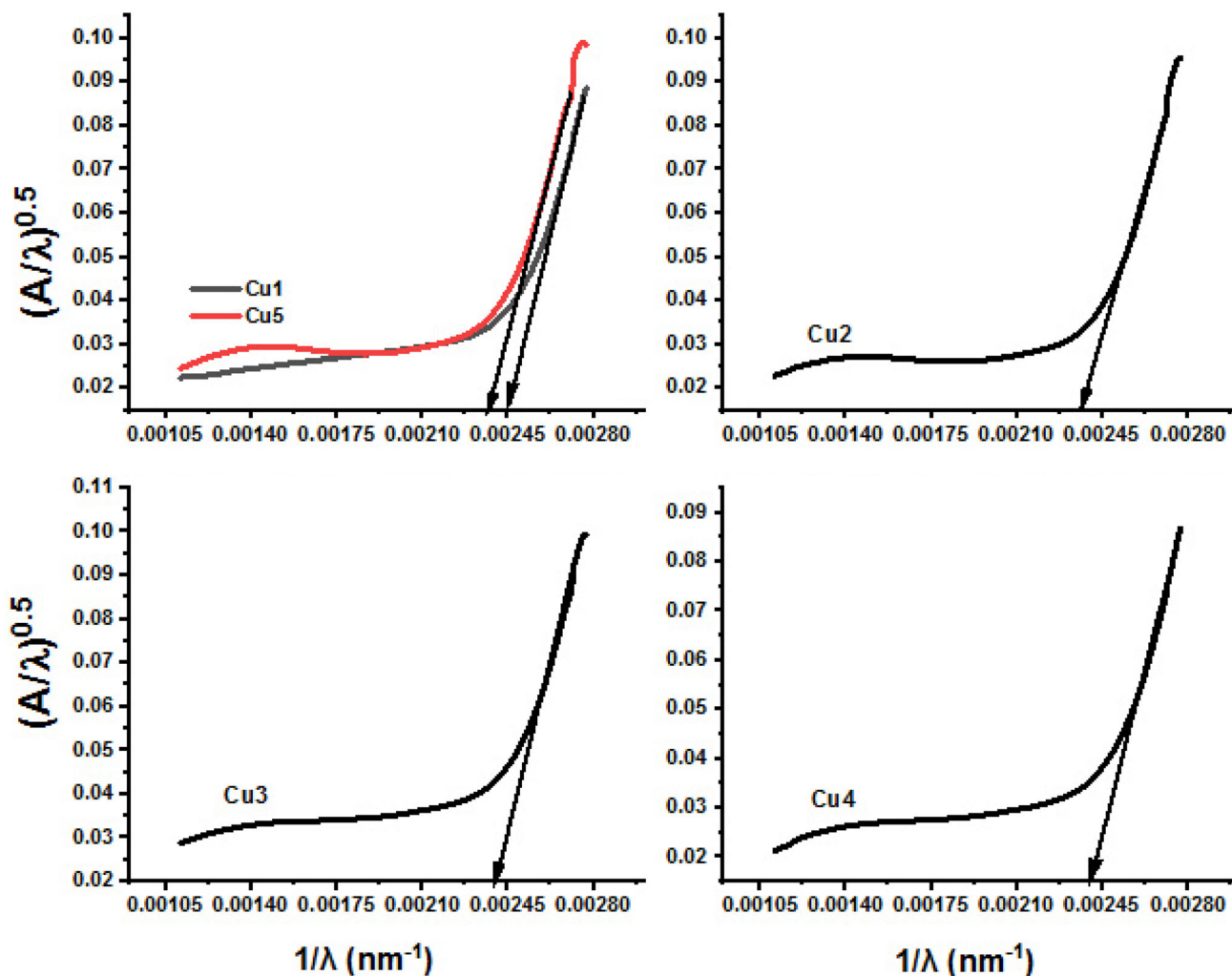


Fig. 8 Dependence of  $(A/\lambda)^{0.5}$  on  $\lambda^{-1}$  for Cu<sub>1</sub>–Cu<sub>5</sub> glasses



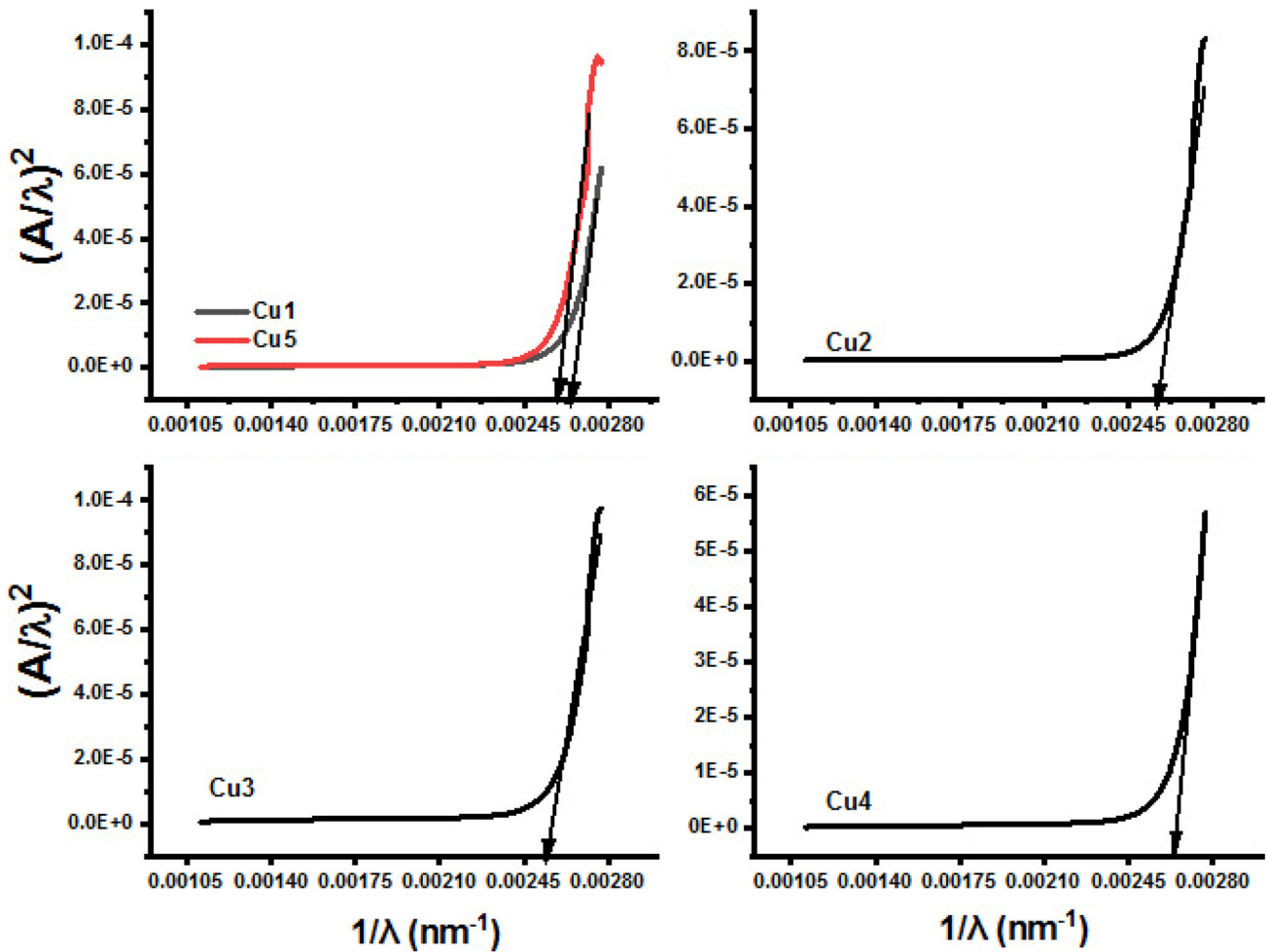


Fig. 9 Dependence of  $(A/\lambda)^2$  on  $\lambda^{-1}$  for Cu<sub>1</sub>–Cu<sub>5</sub> glasses

and indirect allowed transitions was obtained using Eq. (16) [64]:

$$\left(\frac{n^2 - 1}{n^2 + 2}\right) = -1 \sqrt{\frac{E_{opt}}{20}} \tag{16}$$

Table 2 lists the obtained n values for the current samples. The value of optical energy band gaps was inversely proportional to the refractive indices of the samples studied. There is good agreement between values of refractive indices estimated by different methods, as seen in Table 2.

### 3.5 Photoluminescence spectra

The emission spectra of glasses are shown in Fig. 12. There is no emission spectrum detected because the basic glass Cu<sub>1</sub> contains no copper ions. The excitation wavelength affects the intensity of emission

peaks and the position of bands. Figure 12 shows the emission spectra of the Cu-doped glass samples when they are excited at 270 nm. The spectra reveal two main peaks for all samples at about 465 and 510 nm with two shoulders at 420 and 560 nm. It is noted that with increasing CuO concentration above 0.005, the intensity of the emission peaks decreased.

Ultraviolet excitation causes strong and broad emission peaks in copper-doped oxide glasses in the visible range [65, 66], where the excitation bands of the cuprous and cupric ions are placed in UV region. Due to the UV absorption by the oxygen ligands around the cations, oxide-based glasses show charge transfer band in the ultraviolet region, according to the ligand field theory [67]. The present glass samples show emission spectra in the visible region when excited at 270 nm which is due to the charge transfer

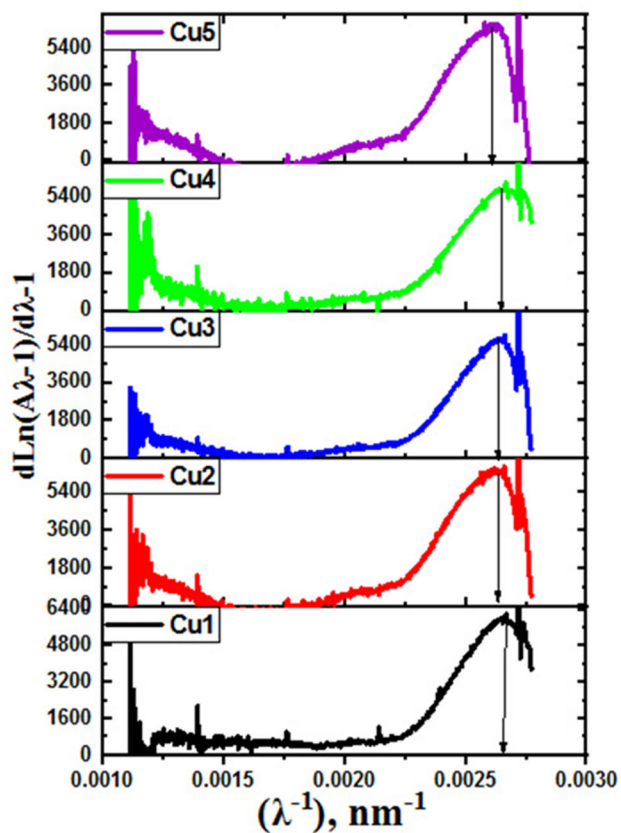


Fig. 10 Variation  $d\{\ln[A(\lambda)/\lambda]\}/d(1/\lambda)$  with  $\lambda^{-1}$  for Cu<sub>1</sub>–Cu<sub>5</sub> glasses

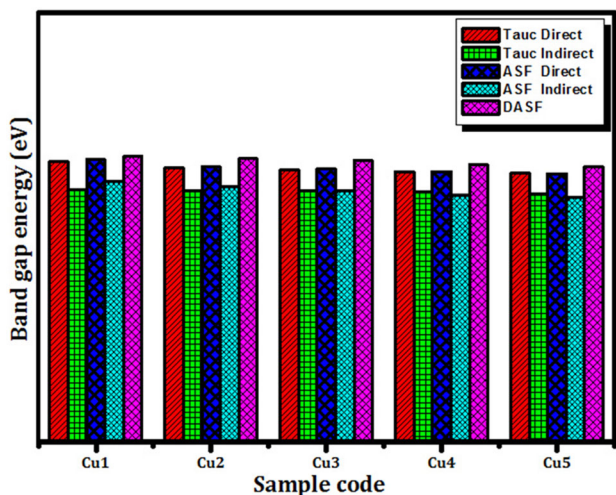


Fig. 11 Comparison of the energy band gaps of the glasses determined by the Tauc, ASF, and DASF methods

process caused by oxygen anions around the copper ions.

Emission peaks and shoulders at 420 and 465 nm can be attributed to  $3d^9 4s^2 \rightarrow 3d^{10}4s^1$  triplet

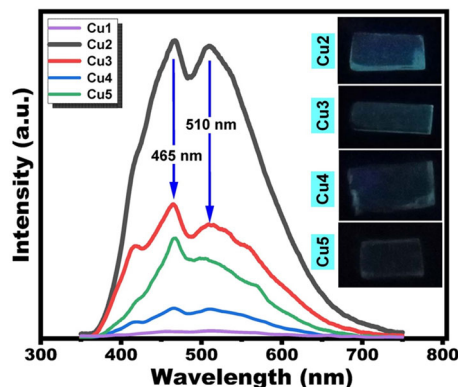


Fig. 12 Photoluminescence emission spectra (excitation at 270 nm) of the prepared glasses

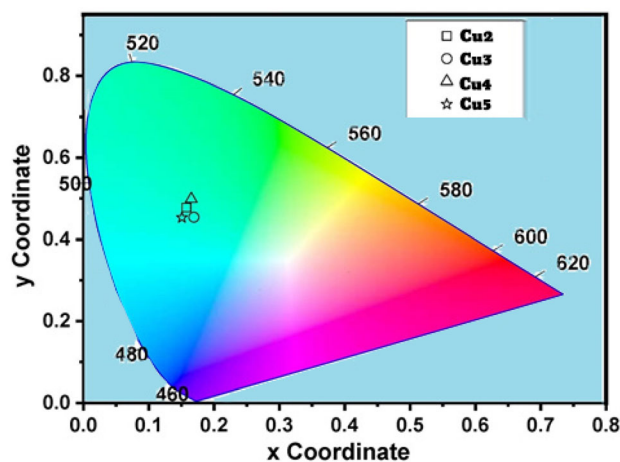
transitions in Cu<sup>2+</sup> ions in the photoluminescence spectrum of CuO-doped glasses [61]. Also, based on the previous studies [68, 69], in an environment with octahedral symmetry, the lowest energy level <sup>3</sup>E<sub>g</sub> of Cu<sup>+</sup> ions is split in the spin–orbit components T<sub>1g</sub> and T<sub>2g</sub>. The emission peaks at about 510 nm and 560 nm can be attributed to the transition between these T<sub>1g</sub> and T<sub>2g</sub> levels to <sup>1</sup>A<sub>g</sub> level ground state of Cu<sup>+</sup> ions, which may be generated from the interaction of NBOs with Cu<sup>2+</sup> ions in the glass samples. Hence, the luminescence spectra reveal the presence of both Cu<sup>2+</sup> and Cu<sup>+</sup> ions, which are responsible both for the observed emission peaks. The electronic excitation energy transfer from Cu<sup>+</sup> to Cu<sup>2+</sup> ions is responsible for the quenching of photoluminescence intensity when CuO content is increased [68]. Another mechanism postulated by Tanaka et al. [19] is absorption caused by a charge transfer from Cu<sup>2+</sup> to O<sup>2-</sup> ions interfering with Cu<sup>+</sup> ions excitation. This mechanism interprets the increase of intensity of the emission peak at 465 nm due to Cu<sup>2+</sup> ions on the expense of that of Cu<sup>+</sup> ions at 510 nm by increasing CuO content.

### 3.6 Chromaticity coordinates

All glass samples had their CIE chromaticity coordinates determined using emission spectra under the excitation of 270 nm. Table 3 lists color coordinates for all glass samples, and Fig. 13 depicts the CIE color chart that corresponds to them. Its color is greenish blue.

**Table 3** CIE coordinates of glass samples with an excitation of 270 nm

Excitation	Coordinate	Glass code			
		Cu <sub>2</sub>	Cu <sub>3</sub>	Cu <sub>4</sub>	Cu <sub>5</sub>
270 nm	x	0.1570	0.1627	0.1536	0.1507
	y	0.4597	0.4541	0.4650	0.4541

**Fig. 13** CIE chromaticity diagram of the prepared glasses

## 4 Conclusions

Homogeneous glasses of zinc borate doped with copper oxide were prepared by the melt–quenching method. Density, FTIR spectroscopy, UV/Vis optical absorption, and photoluminescence spectroscopy were used to analyze the glass samples. The density decreases from 3.9318 to 3.8474 g/cm<sup>3</sup> with the addition of CuO. The analysis of FTIR results suggests that the glass consists of BO<sub>3</sub>, BO<sub>4</sub>, and ZnO<sub>4</sub> bridge bonds, forming a large glass matrix. The transformation from [BO<sub>4</sub>] tetrahedral to [BO<sub>3</sub>] triangular occurs as CuO content increases. Due to Cu<sup>2+</sup> ion <sup>2</sup>B<sub>1g</sub> → <sup>2</sup>B<sub>2g</sub> transitions, the UV–Vis absorption spectra of these glasses exhibit a single broad band. This demonstrates that the cupric ions occupy distorted octahedral positions. Tauc, ASF, and DASf methods were used to investigate changes in optical band gap energies (E<sub>g</sub>). The conclusion is that the three techniques provide results that are extremely similar. The optical absorption spectra the E<sub>g</sub><sup>opt</sup> have been examined glasses decrease with the

addition of copper ions due to structural changes. Emission spectra displayed emission bands owing to Cu<sup>2+</sup> ions. CIE chromaticity diagram shows glass sample Cu<sub>2</sub> with color coordinates  $x = 0.1570$  and  $y = 0.4597$  have highest emission intensity. Analysis of CIE color coordinates illustrates that the CuO co-doped multicomponent glasses emit greenish blue light. These results suggest that the prepared glasses can be useful for the photonics applications.

## Author contributions

SI: Conceptualization, Methodology, Validation, Investigation, Data curation, Writing—original draft, and Writing—review and editing. YH: Conceptualization, Methodology, Validation, Investigation, Data curation, Writing—original draft, and Writing—review and editing. HD: Conceptualization, Methodology, Validation, Investigation, Data curation, Writing—original draft, and Writing—review and editing. AAA: Conceptualization, Methodology, Validation, Investigation, Data curation, Writing—original draft, and Writing—review and editing.

## Funding

Open access funding provided by The Science, Technology & Innovation Funding Authority (STDF) in cooperation with The Egyptian Knowledge Bank (EKB). The authors have not disclosed any funding.

## Data availability

The datasets generated during and/or analyzed during the current study are available from the corresponding author on reasonable request.

## Declarations

**Conflict of interest** The authors have not disclosed any competing interests.

**Ethical approval** This article does not contain any studies involving animals performed by any of the authors.

**Open Access** This article is licensed under a Creative Commons Attribution 4.0 International License, which permits use, sharing, adaptation, distribution and reproduction in any medium or format, as long as you give appropriate credit to the original author(s) and the source, provide a link to the Creative Commons licence, and indicate if changes were made. The images or other third party material in this article are included in the article's Creative Commons licence, unless indicated otherwise in a credit line to the material. If material is not included in the article's Creative Commons licence and your intended use is not permitted by statutory regulation or exceeds the permitted use, you will need to obtain permission directly from the copyright holder. To view a copy of this licence, visit <http://creativecommons.org/licenses/by/4.0/>.

## References

- G.N. Raju, M.S. Reddy, K.S.V. Sudhakar, N. Veeraiah, Spectroscopic properties of copper ions in ZnO–ZnF<sub>2</sub>–B<sub>2</sub>O<sub>3</sub> glasses. *Opt. Mater.* **29**(11), 1467–1474 (2007). <https://doi.org/10.1016/j.optmat.2006.07.006>
- L. Zhou, H. Lin, W. Chen, L. Lua, IR and Raman investigation on the structure of (100–x)B<sub>2</sub>O<sub>3</sub>–x[0.5BaO–0.5ZnO] glasses. *J. Phys. Chem. Solids* **69**(10), 2499–2502 (2008). <https://doi.org/10.1016/j.ceramint.2011.05.134>
- P. Pascuta, E. Culea, Structural and thermal properties of some zinc borate glasses containing gadolinium ions. *J. Mater. Sci. Mater. Electron.* **22**(8), 1060–1066 (2011). <https://doi.org/10.1007/s10854-010-0259-8>
- M.S. Gaafar, N.S. Abd El-Aal, O.W. Gerges, G. El-Amir, Elastic properties and structural studies on some zinc-borate glasses derived from ultrasonic, FT-IR and X-ray techniques. *J. Alloys Compd.* **475**, 535–542 (2009). <https://doi.org/10.1016/j.jallcom.2008.07.114>
- Y. Gandhi, N. Purnachand, K.S.V. Sudhakar, T. Satyanarayana, N. Veeraiah, Influence of modifier oxides on some physical properties of antimony borate glass system doped with V<sub>2</sub>O<sub>5</sub>. *Mater. Chem. Phys.* **120**(1), 89–97 (2010). <https://doi.org/10.1016/j.matchemphys.2009.10.026>
- A. Saidu, H. Wagiran, M.A. Saeed, H.K. Obayes, A. Bala, F. Usman, Thermoluminescence response of rare earth activated zinc lithium borate glass. *Radiat. Phys. Chem.* **144**, 413–418 (2018). <https://doi.org/10.1016/j.radphyschem.2017.10.004>
- M.N. Azlan, M.K. Halimah, H.A.A. Sidek, Linear and non-linear optical properties of erbium doped zinc borotellurite glass system. *J. Lumin.* **181**, 400–406 (2017). <https://doi.org/10.1016/j.jlumin.2016.09.047>
- N.J. Kreidl, Recent applications of glass science. *J. Non-Cryst. Solids* **123**(1–3), 377–384 (1990)
- K. Srinivasulu, I. Omkaram, H. Obeid, A. Suresh Kumar, J.L. Rao, Spectral studies on Cu<sup>2+</sup> ions in sodium–lead borophosphate glasses. *Physica B* **407**(24), 4741–4748 (2012). <https://doi.org/10.1016/j.physb.2012.09.010>
- A. Durán, J.F. Navarro, The colouring of glass by Cu<sup>2+</sup> ions. *Phys. Chem. Glasses* **26**, 126 (1985)
- C.R. Bamford, The application of the ligand field theory to coloured glasses. *Phys. Chem. Glasses* **3**, 189–202 (1962)
- G. Lakshminarayana, S. Buddhudu, Spectral analysis of Cu<sup>+</sup>:B<sub>2</sub>O<sub>3</sub>–ZnO–PbO glasses. *Spectrochim. Acta A* **62**, 364–371 (2005). <https://doi.org/10.1016/j.saa.2005.01.014>
- I. Ardelean, S. Cora, V. Ioncu, Structural investigation of CuO–Bi<sub>2</sub>O<sub>3</sub>–B<sub>2</sub>O<sub>3</sub> glasses by FT-IR, Raman and UV–Vis spectroscopies. *J. Optoelectron. Adv. Mater.* **8**(5), 1843–1847 (2006)
- P. Ramesh Babu, R. Vijay, P. Srinivasa Rao, P. Suresh, N. Veeraiah, D. Krishna Rao, Dielectric and spectroscopic properties of CuO doped multi-component Li<sub>2</sub>O–PbO–B<sub>2</sub>O<sub>3</sub>–SiO<sub>2</sub>–Bi<sub>2</sub>O<sub>3</sub>–Al<sub>2</sub>O<sub>3</sub> glass system. *J. Non-Cryst. Solids* **370**, 21–30 (2013). <https://doi.org/10.1016/j.jnoncrysol.2013.03.026>
- J.A. Jiménez, Luminescent properties of Cu<sup>+</sup>/Sn<sup>2+</sup>-activated aluminophosphate glass. *Opt. Mater.* **37**, 347–351 (2014). <https://doi.org/10.1016/j.optmat.2014.06.024>
- W. Xiang, H. Gao, L. Ma, X. Ma, Y. Huang, L. Pei, X. Liang, Valence state control and third-order nonlinear optical properties of copper embedded in sodium borosilicate glass. *ACS Appl. Mater. Interfaces* **7**, 10162–10168 (2015). <https://doi.org/10.1021/acsami.5b00218>
- N. Aboufotouh, Y. El Bashar, M. Ibrahim, M. Elokr, Characterization of copper doped phosphate glasses for optical applications. *Ceram. Int.* **40**(7), 10395–10399 (2014)
- J.A. Jiménez, Efficient Cu<sup>+</sup> to Ho<sup>3+</sup> energy transfer in highly CuO/SnO codoped phosphate glass. *J. Inorg. Organomet. Polym.* **28**, 352–357 (2018). <https://doi.org/10.1007/s10904-017-0696-4>
- K. Tanaka, T. Yano, S. Shibata, M. Yamane, S. Inoue, Cu<sup>+</sup>-doped CaO–P<sub>2</sub>O<sub>5</sub> glasses for lasers. *J. Non-Cryst. Solids* **178**, 9–14 (1994). [https://doi.org/10.1016/0022-3093\(94\)90258-5](https://doi.org/10.1016/0022-3093(94)90258-5)
- A. Samir, M.A. Hassan, A. Abokhadra, L.I. Soliman, M. Elokr, Characterization of borate glasses doped with copper oxide for optical application. *Opt. Quantum Electron.* **51**, 123 (2019). <https://doi.org/10.1007/s11082-019-1819-7>
- J.C. Zhang, B. Moine, C. Pedrini, C. Parent, G. Flem, Optical spectroscopy of monovalent copper-doped borate glasses.



- J. Phys. Chem. Solids **51**(8), 933–939 (1990). [https://doi.org/10.1016/0022-3697\(90\)90035-E](https://doi.org/10.1016/0022-3697(90)90035-E)
22. J.W.M. Verwey, J.M. Coronado, G. Blasse, The luminescence of Cu(I) in strontium tetraborate. *J. Solid State Chem.* **92**(2), 531–536 (1991). [https://doi.org/10.1016/0022-4596\(91\)90359-P](https://doi.org/10.1016/0022-4596(91)90359-P)
  23. A. Okasha, S.Y. Marzouk, A.M. Abdelghany, Design a tunable glasses optical filters using CuO doped fluoroborate glasses. *Opt. Laser Technol.* **137**, 106829 (2021). <https://doi.org/10.1016/j.optlastec.2020.106829>
  24. S. Inaba, S. Fujino, Empirical equation for calculating the density of oxide. *J. Am. Ceram. Soc.* **93**(1), 217–220 (2010). <https://doi.org/10.1111/j.1551-2916.2009.03363.x>
  25. S. Ibrahim, S.M. Abo-Naf, M.A. Marzouk, Photoluminescence behavior of nano-structured sol-gel prepared zinc oxide activated with manganese and/or chromium ions. *J. Mater. Sci. Mater. Electron.* **32**, 15491 (2021). <https://doi.org/10.1007/s10854-021-06098-9>
  26. D. Malacara, *Color Vision and Colorimetry; Theory and Applications*, 2nd edn. (SPIE Press, Bellingham, 2011). <https://doi.org/10.1117/3.881172>
  27. R.J. Mortimer, T.S. Varley, Quantification of colour stimuli through the calculation of CIE chromaticity coordinates and luminance data for application to in situ colorimetry studies of electrochromic materials. *Displays* **32**, 35–44 (2011). <https://doi.org/10.1016/j.displa.2010.10.001>
  28. Y.S. Rammah, I.O. Olarinoy, F.I. El-Agawany, S. El Sayed Yousef, A.A.A. Ibrahim, SrO-reinforced potassium sodium borophosphate bioactive glasses: compositional, physical, spectral, structural properties and photon attenuation competence. *J. Non-Cryst. Solids* **559**, 1206673 (2021). <https://doi.org/10.1016/j.jnoncrysol.2021.120667>
  29. R. Stefan, E. Culea, P. Pascuta, The effect of copper ions addition on structural and optical properties of zinc borate glasses. *J. Non-Cryst. Solids* **358**, 839–846 (2012). <https://doi.org/10.1016/j.jnoncrysol.2011.12.079>
  30. M. Farouk, A. Samir, M. El Okr, Effect of alkaline earth modifier on the optical and structural properties of Cu<sup>2+</sup> doped phosphate glasses as a bandpass filter. *Physica B* **530**, 43–48 (2018). <https://doi.org/10.1016/j.physb.2017.11.013>
  31. G. Naga Raju, N. Veeraiah, G. Nagarjuna, P.V.V. Satyanarayana, The structural role of chromium ions on the improvement of insulating character of ZnO–ZnF<sub>2</sub>–B<sub>2</sub>O<sub>3</sub> glass system by means of dielectric, spectroscopic and magnetic properties. *J. Phys. B* **373**(2), 297 (2006). <https://doi.org/10.1016/j.physb.2005.11.164>
  32. S. Bale, S. Rahman, A.M. Awasthi, V. Sathe, Role of Bi<sub>2</sub>O<sub>3</sub> Content on physical, optical and vibrational studies in Bi<sub>2</sub>O<sub>3</sub>–ZnO–B<sub>2</sub>O<sub>3</sub> glasses. *J. Alloys Compd.* **460**, 699–703 (2008). <https://doi.org/10.1016/j.jallcom.2007.06.090>
  33. L. Zhou, H. Lin, W. Chen, L. Luo, IR and Raman investigation on the structure of (100–x)B<sub>2</sub>O<sub>3</sub>–x[0.5BaO–0.5ZnO] glasses. *J. Phys. Chem. Solids* **69**(10), 2499–2502 (2008). <https://doi.org/10.1016/j.jpcs.2008.05.013>
  34. P. Pascuta, Structural investigations of some bismuth–borate–vanadate glasses doped with gadolinium ions. *J. Mater. Sci. Mater. Electron.* **21**, 338–342 (2010). <https://doi.org/10.1007/s10854-009-9917-0>
  35. Y. Saddeek, Structural and acoustical studies of lead sodium borate glasses. *J. Alloys Compd.* **467**, 14–21 (2009). <https://doi.org/10.1016/j.jallcom.2007.11.126>
  36. A. Ramesh Babu, S. Yusub, Ascendancy of iron ions on lithium ion conductivity, optical band gap, Urbach energy and topology of LiF–SrO–B<sub>2</sub>O<sub>3</sub> glasses. *J. Non-Cryst. Solids* **533**, 119906 (2020). <https://doi.org/10.1016/j.jnoncrysol.2020.119906>
  37. I. Pal, A. Agarwal, S. Sanghi, M.P. Aggarwal, Structure and optical absorption of Sm<sup>3+</sup> and Nd<sup>3+</sup> ions in cadmium bismuth borate glasses with large radiative transition probabilities. *Opt. Mater.* **34**(7), 1171–1180 (2012). <https://doi.org/10.1016/j.optmat.2012.01.023>
  38. B. Sumalatha, I. Omkaram, T.R. Rao, C.L. Raju, Alkaline earth zinc borate glasses doped with Cu<sup>2+</sup> ions studied by EPR, optical and IR techniques. *J. Non-Cryst. Solids* **357**(16, 17), 3143–3152 (2011). <https://doi.org/10.1016/j.jnoncrysol.2011.05.005>
  39. P.W. France, S.F. Carter, J.M. Parker, Oxidation states of 3d transition metals in ZrF<sub>4</sub> glasses. *Phys. Chem. Glasses* **27**(1), 32–41 (1986)
  40. Y. Cheng, H. Xiao, G. Wenming, G. Weiming, Structure and crystallization kinetics of Bi<sub>2</sub>O<sub>3</sub>–B<sub>2</sub>O<sub>3</sub> glasses. *Thermochim. Acta* **444**(2), 173–178 (2006). <https://doi.org/10.1016/j.tca.2006.03.016>
  41. S. Bale, S. Rahmana, A.M. Awasthi, V. Sathe, Role of Bi<sub>2</sub>O<sub>3</sub> content on physical, optical and vibrational studies in Bi<sub>2</sub>O<sub>3</sub>–ZnO–B<sub>2</sub>O<sub>3</sub> glasses. *J. Alloys Compd.* **460**(1–2), 699–703 (2008). <https://doi.org/10.1016/j.jallcom.2007.06.090>
  42. P. Subbalakshmi, N. Veeraiah, Influence of WO<sub>3</sub> on dielectric properties of zinc phosphate glasses. *Indian J. Eng. Mater. Sci.* **8**, 275–284 (2001)
  43. M. Shaaban, I. Salem, Shaltout, Structure, electrical, and optical properties of ZnO-substituted PbO for the Er<sup>3+</sup>/Yb<sup>3+</sup> co-doped Bi<sub>2</sub>O<sub>3</sub>–GeO<sub>2</sub>–Na<sub>2</sub>O glass system. *J. Mater. Sci.* **45**, 1837–1845 (2010). <https://doi.org/10.1007/s10853-009-4167-3>
  44. S.M. Salem, E.M. Antar, E.A. Mohamed, Structural and dielectric properties of Li<sub>2</sub>O–ZnO–BaO–B<sub>2</sub>O<sub>3</sub>–CuO glasses. *J. Mater. Sci.* **46**, 1095–1102 (2011)
  45. V. Aruna, S. Yusubb, M. Venkateswarlu, A. Ramesh Babu, K. Anith, Efficacy of copper ions on lithium ion conductivity,



- electron hopping, optical band gap, metallization criterion and morphology of  $\text{Li}_2\text{O}-\text{B}_2\text{O}_3-\text{P}_2\text{O}_5$  glasses. *J. Non-Cryst. Solids* **536**, 120015 (2020). <https://doi.org/10.1016/j.jnoncrysol.2020.120015>
46. S. Cetinkaya Colak, E. Aral, Optical and thermal properties of  $\text{P}_2\text{O}_5-\text{Na}_2\text{O}-\text{CaO}-\text{Al}_2\text{O}_3:\text{CoO}$  glasses doped with transition metals. *J. Alloys Compd.* **509**, 4935–4939 (2011). <https://doi.org/10.1016/j.jallcom.2011.01.172>
  47. T.H. Noh, E.L. Shim, Study of CuO content on physical and structural properties of  $\text{Li}_2\text{O}-\text{B}_2\text{O}_3-\text{CuO}$  glasses using electron paramagnetic resonance. *J. Non-Cryst. Solids* **474**, 37–42 (2017). <https://doi.org/10.1016/j.jnoncrysol.2017.08.021>
  48. V. Ramesh Kumar, J.L. Rao, N.O. Gopal, EPR and optical absorption studies of  $\text{Cu}^{2+}$  ions in alkaline earth aluminoborate glasses. *Mater. Res. Bull.* **40**(8), 1256–1269 (2005). <https://doi.org/10.1016/j.materresbull.2005.04.010>
  49. L. Srinivasa Rao, M. Srinivasa Reddy, D. Krishna Rao, N. Veeraiah, Influence of redox behavior of copper ions on dielectric and spectroscopic properties of  $\text{Li}_2\text{O}-\text{MoO}_3-\text{B}_2\text{O}_3:\text{CuO}$  glass system. *Solid State Sci.* **11**(2), 578–587 (2009). <https://doi.org/10.1016/j.solidstatesciences.2008.06.022>
  50. J. Tauc (ed.), *Amorphous and Liquid Semiconductors*. (Plenum Press, New York, 1974)
  51. N.F. Mott, E.A. Davies, *Electronic Processes in Non-crystalline Materials* (Clarendon Press, Oxford, 1979)
  52. D. Souri, K. Shomalian, Band gap determination by absorption spectrum fitting method (ASF) and structural properties of different compositions of  $(60-x)\text{V}_2\text{O}_5-40\text{TeO}_2-x\text{Sb}_2\text{O}_3$  glasses. *J. Non-Cryst. Solids* **355**, 1597–1601 (2009). <https://doi.org/10.1016/j.jnoncrysol.2009.06.003>
  53. D. Souri, Z.E. Tahan, A new method for the determination of optical band gap and the nature of optical transitions in semiconductors. *Appl. Phys. B* **119**, 273–279 (2015). <https://doi.org/10.1007/s00340-015-6053-9>
  54. L.E. Alarcon, A. Arrieta, E. Camps, S. Muhl, S. Rudil, E.V. Santiago, An alternative procedure for the determination of the optical band gap and thickness of amorphous carbon nitride thin films. *Appl. Surf. Sci.* **254**, 412–415 (2007). <https://doi.org/10.1016/j.apsusc.2007.07.052>
  55. A.A. Ali, Y.S. Rammah, R. El-Mallawany, D. Souri, FTIR and UV spectra of pentatertiary borate glasses. *Measurement* **105**, 72–77 (2017). <https://doi.org/10.1016/j.measurement.2017.04.010>
  56. Ö.B. Mergen, E. Arda, Determination of optical band gap energies of CNT bio-nanocomposites by Tauc and ASF methods. *Synth. Met.* **269**, 116539 (2020). <https://doi.org/10.1016/j.synthmet.2020.116539>
  57. S.K.J. Al-Ani, Determination of the optical gap of amorphous materials. *Int. J. Electron.* **75**, 1153–1163 (1993). <https://doi.org/10.1080/00207219308907191>
  58. F.A. Davis, N.F. Mott, Conduction in non-crystalline systems V. Conductivity, optical absorption and photoconductivity in amorphous semiconductors. *Philos. Mag.* **22**(179), 0903–0922 (1970). <https://doi.org/10.1080/14786437008221061>
  59. J. Tauc, A. Menth, States in the gap. *J. Non-Cryst. Solids* **8–10**, 569–585 (1972). [https://doi.org/10.1016/0022-3093\(72\)90194-9](https://doi.org/10.1016/0022-3093(72)90194-9)
  60. C.K. Jorgensen, Recent progress in ligand field theory. *Acta Chem. Scand.* **11**, 73 (1957)
  61. Ch. Rajyasree, P. Michael Vinaya Teja, K.V.R. Murthy, D. Krishna Rao, Optical and other spectroscopic studies of lead, zinc bismuth borate glasses doped with CuO. *Physica B* **406**(23), 4366–4372 (2011). <https://doi.org/10.1016/j.physb.2011.08.082>
  62. Y. Shahmoradi, D. Souri, Growth of silver nanoparticles within the tellurovanadate amorphous matrix: optical band gap and band tailing properties, beside the Williamson-Hall estimation of crystallite size and lattice strain. *Ceram. Int.* **45**(6), 7857–7864 (2019). <https://doi.org/10.1016/j.ceramint.2019.01.094>
  63. S.H. Elazoumi, H.A.A. Sidek, Y.S. Rammah, R. El-Mallawany, M.K. Halimah, K.A. Matori, M.H.M. Zaid, Effect of PbO on optical properties of tellurite glass. *Results Phys.* **8**, 16–25 (2018). <https://doi.org/10.1016/j.rinp.2017.11.010>
  64. V. Dimitrov, S. Sakka, Electronic oxide polarizability and optical basicity of simple oxides. *J. Appl. Phys.* **79**, 1736–1740 (1996)
  65. A. Yasumori, F. Tada, S. Yanagida, T. Kishi, Yellow photoluminescence properties of copper ion doped phase-separated glasses in alkali borosilicate system. *J. Electrochem. Soc.* **159**(5), J143–J147 (2012)
  66. J.A. Jimenez, Efficient stabilization of  $\text{Cu}^+$  ions in phosphate glasses via reduction of  $\text{Cu}^{2+}$  by  $\text{Sn}^{2+}$  during ambient atmosphere melting. *J. Mater. Sci.* **49**, 4387–4393 (2014). <https://doi.org/10.1007/s10853-014-8138-y>
  67. B.N. Figgis, *Introduction to Ligand Field Theory* (Wiley, New York, 1966)
  68. E. Borsella, A. Dal Vecchio, M.A. Garcia, C. Sada, F. Gonella, R. Polloni, A. Quaranta, L.J.G.W. van Wilderen, Copper doping of silicate glasses by the ion-exchange technique: a photoluminescence spectroscopy study. *J. Appl. Phys.* **91**(1), 90–98 (2002). <https://doi.org/10.1063/1.1421241>

69. J. Ramkumar, V. Sudarsan, S. Chandramouleeswaran, V.K. Shrikhande, G.P. Kothiyal, P.V. Ravindran, S.K. Kulshreshtha, T. Mukherjee, Structural studies on boroaluminosilicate glasses. *J. Non-Cryst. Solids* **354**(15–16), 1591–1597 (2008). <https://doi.org/10.1016/j.jnoncrysol.2007.10.005>

**Publisher's Note** Springer Nature remains neutral with regard to jurisdictional claims in published maps and institutional affiliations.